

Supporting Information

Inhibiting Shuttle Effect by Artificial Membranes with High Lithium-ion Content for Enhancing the Stability of Lithium Anode

Dong Liang, Tengfei Bian, Qing Han, Hua Wang, Xiaosheng Song, Binbin Hu, Jinling He*, Yong Zhao**

Supporting Figures

Figure S1

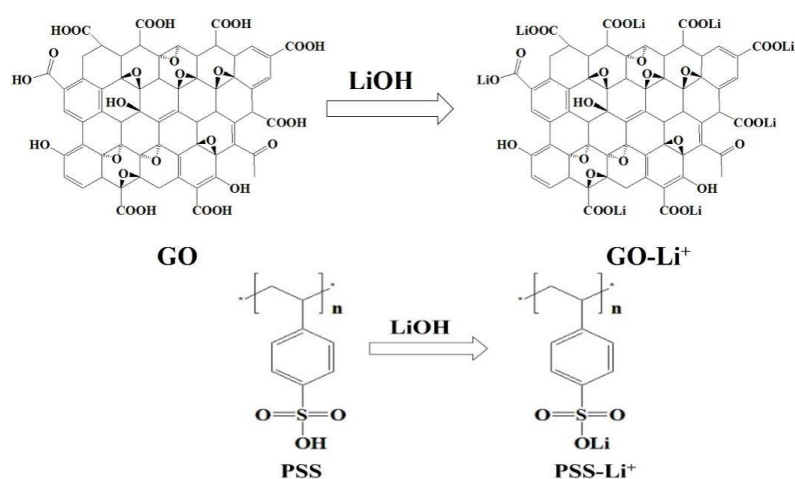


Figure S1 Synthesis procedures of lithiated graphene oxide (GO-Li) and lithiated poly(styrene sulfonate) (PSS-Li).

Figure S2

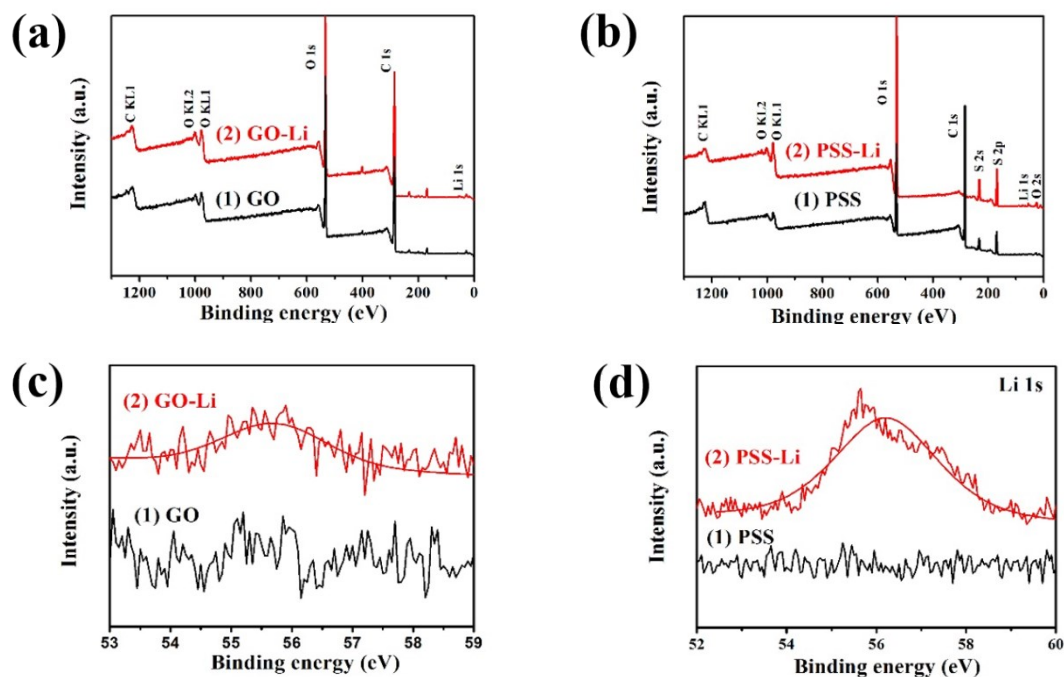


Figure S2 XPS full spectra of (a) lithiated graphene oxide (GO-Li) and GO, (b) lithiated poly(styrene sulfate) (PSS-Li) and PSS. XPS Li 1s spectra of (c) lithiated graphene oxide (GO-Li) and GO, (d) poly(styrene sulfate) (PSS-Li) and PSS.

Table 1 The elemental content of lithiated graphene oxide (GO-Li), GO, poly(styrene sulfate) (PSS-Li) and PSS from XPS analysis.

Sample	C	O	Li
GO	69.7%	30.3%	0.0%
GO-Li	67.0%	28.5%	4.5%

Sample	C	O	S	Li
PSS	74.4%	18.9%	6.7%	0.0%
PSS-Li	26.7%	39.2%	11.1%	23.0%

Figure S3

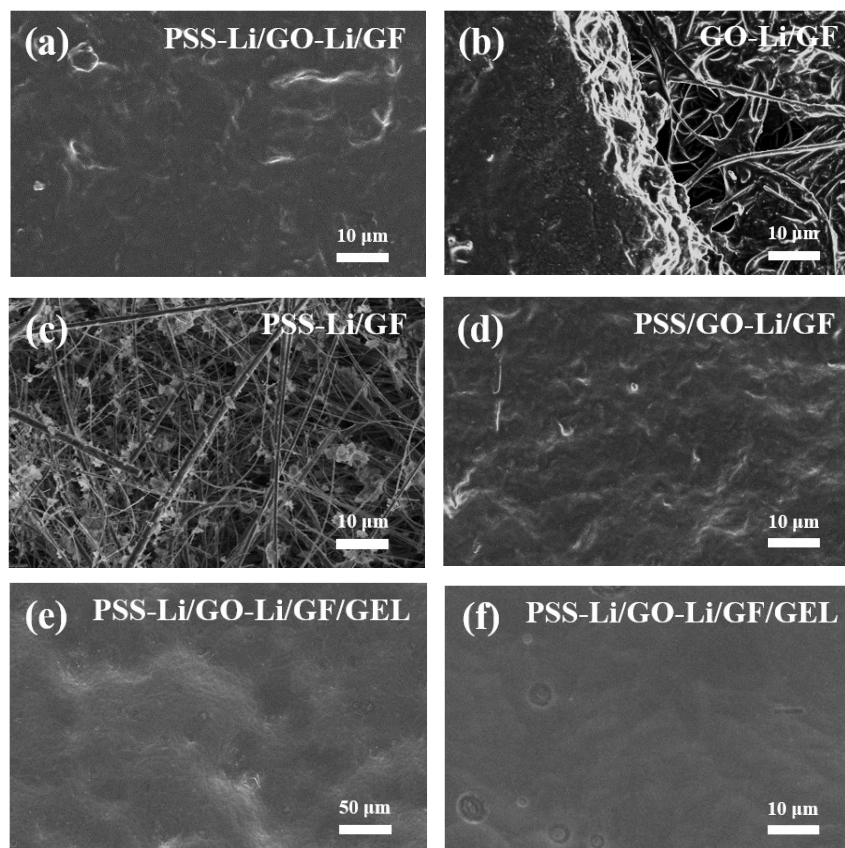


Figure S3 Surface morphologies of (a) PSS-Li/GO-Li/GF, (b) GO-Li/GF, (c) PSS-Li/GF, (d) PSS/GO-Li/GF, and (e, f) PSS-Li/GO-Li/GF/GEL membranes. Large pores were remained in PSS-Li/GF and GO-Li/GF membranes, while the uniform and dense PSS/GO-Li/GF and PSS-Li/GO-Li/GF membrane were formed.

Figure S4

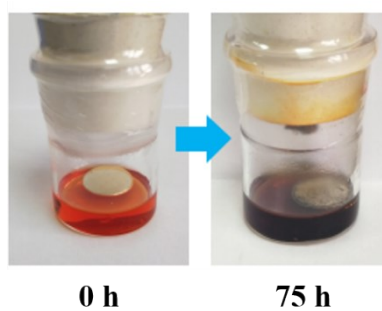


Figure S4 The optical images of Li-metal in the TEMPO-based electrolyte before and after 75 h.

Figure S5

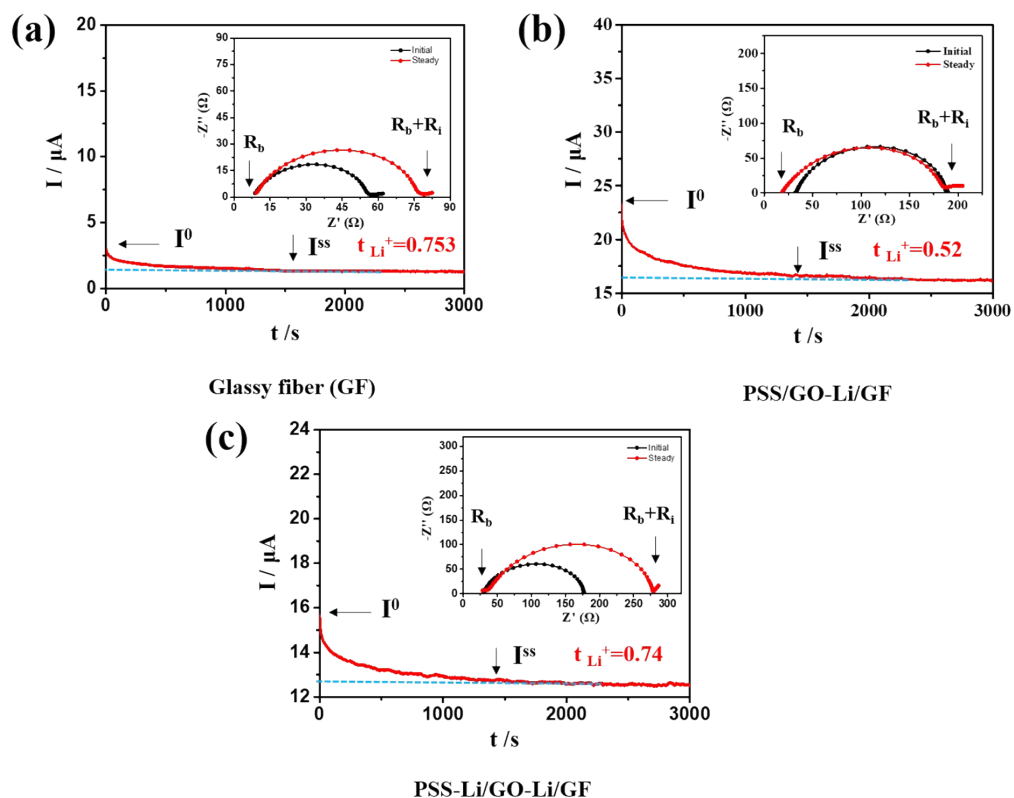


Figure S5 The chronoamperometry profiles of Li||Li symmetric cells with (a) GF, PSS/GO-Li/GF and PSS-Li/GO-Li/GF were tested under a polarization voltage of 10 mV, and the corresponding EIS before and after polarization was provided in the inset.

Figure S6

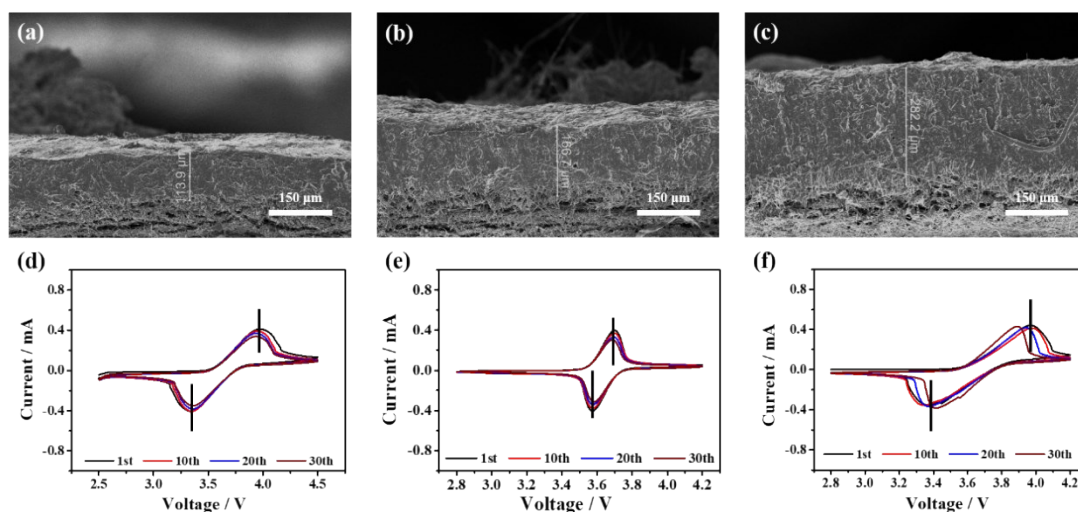


Figure S6 SEM images of PSS-Li/GO-Li/GF membranes with (a) thinner membrane ($\sim 114 \mu\text{m}$). (b) thick membrane ($\sim 167 \mu\text{m}$). (c) thicker membrane ($282 \mu\text{m}$). Cyclic voltammetry of Li||C unsymmetrical cells containing 0.05 M TEMPO with different thicknesses of membranes (d) thinner membranes ($\sim 114 \mu\text{m}$). (e) thick membranes ($\sim 167 \mu\text{m}$). (f) thicker membranes ($\sim 282 \mu\text{m}$). CVs were carried out at a sweep rate of 2 mV/s under Ar atmosphere.

Figure S7

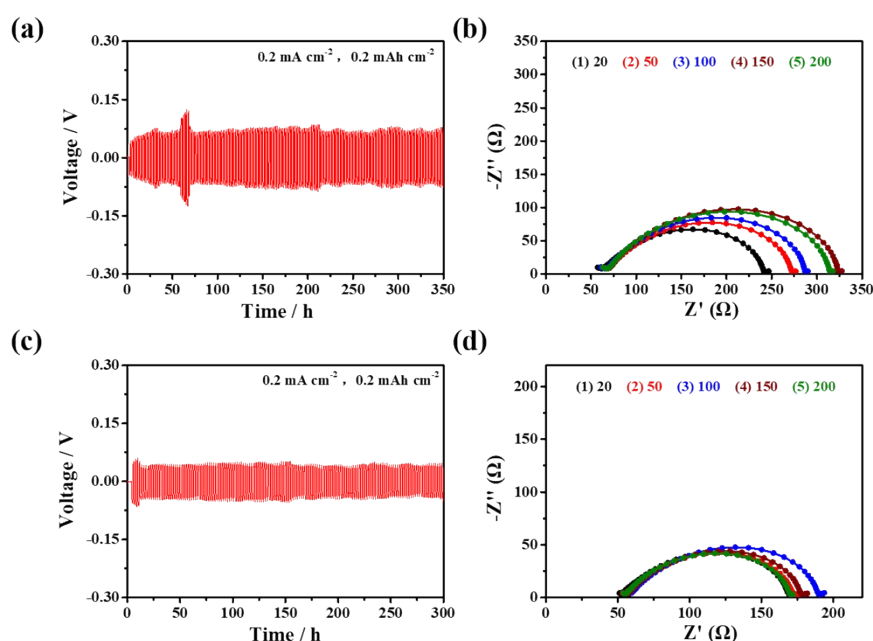


Figure S7 Time-voltage polarization curves with (a) thinner membranes ($\sim 114 \mu\text{m}$) and (c) thicker membranes ($\sim 282 \mu\text{m}$). Nyquist impedance tests of Li||Li symmetrical cell with (b) thinner membranes and (d) thicker membranes.

Note: In the cyclic voltammetry test of Li||C unsymmetrical batteries with the thinner membranes (Fig. S6a, $\sim 114 \mu\text{m}$), the inhibition effect of redox molecules diffusion is weak, and the peak currents continue to decay as the cycle increases (Fig. S6d). The polarization potentials are also larger than the normal thickness of PSS-Li/GO-Li/GF membranes (Fig. S6b, $\sim 167 \mu\text{m}$). With the thicker membranes (Fig. S6c, $\sim 282 \mu\text{m}$), the inhibition effect of TEMPO diffusion was promoted to stabilize the peak current attenuation, but the increase in the thickness of membranes also causes the reduction of Li^+ conductivity, and the polarization potentials is also increased (Fig. S6f). In the test

of lithium symmetrical battery and Nyquist impedance, the thin membrane ($\sim 114 \mu\text{m}$) shows that the polarization voltage and resistance values increase with time (Fig. S7a, S7b). In contrast, With the thicker membranes (Fig. S6c, $\sim 282 \mu\text{m}$), the inhibition effect of TEMPO diffusion was promoted to stabilize the peak current attenuation, but the increase in the thickness of membranes also causes the reduction of Li^+ conductivity, and the polarization potentials is also increased (Fig. S6f, S7d).”

Figure S8

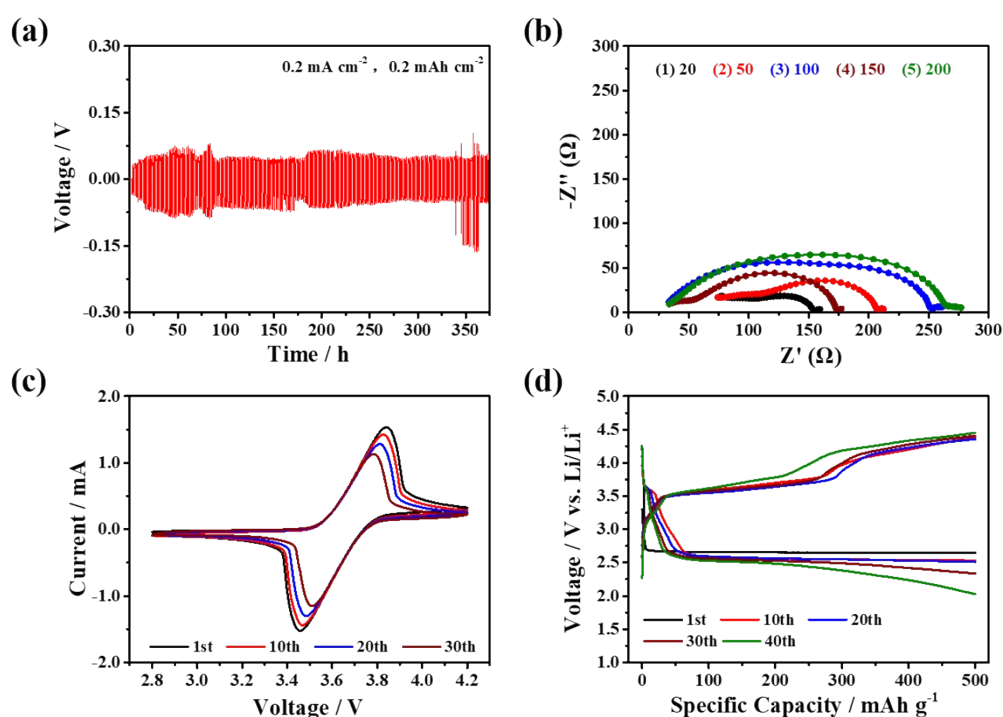


Figure S8 (a) Time-polarization and (b) Nyquist impedance tests of $\text{Li}|\text{Li}$ symmetrical cell with PSS/GO/GF membranes. (c) Cyclic voltammetry of $\text{Li}|\text{C}$ unsymmetrical cells containing 0.05 M TEMPO in the electrolyte with PSS/GO/GF membranes. (d) Cycling performance of Li-O_2 batteries with PSS/GO/GF membranes at a 400 mA g^{-1} under a capacity cut-off of 500 mAh g^{-1} .

Figure S9

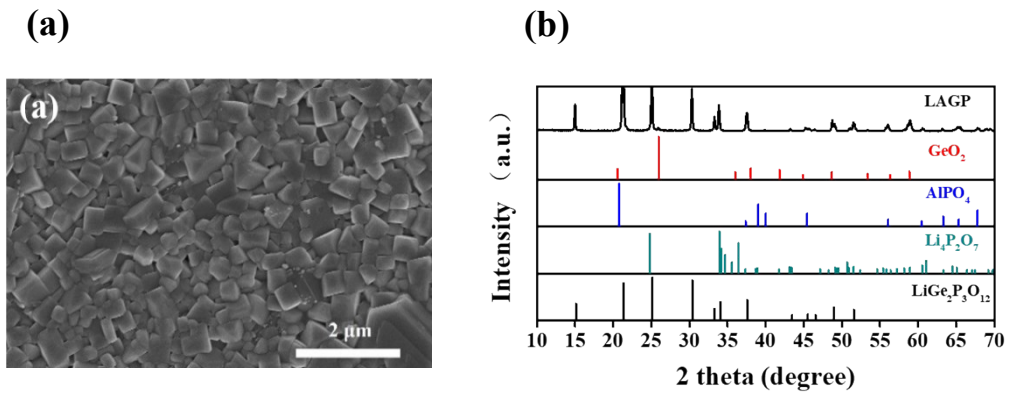


Figure S9 SEM image and XRD pattern of LAGP membranes.

Figure S10

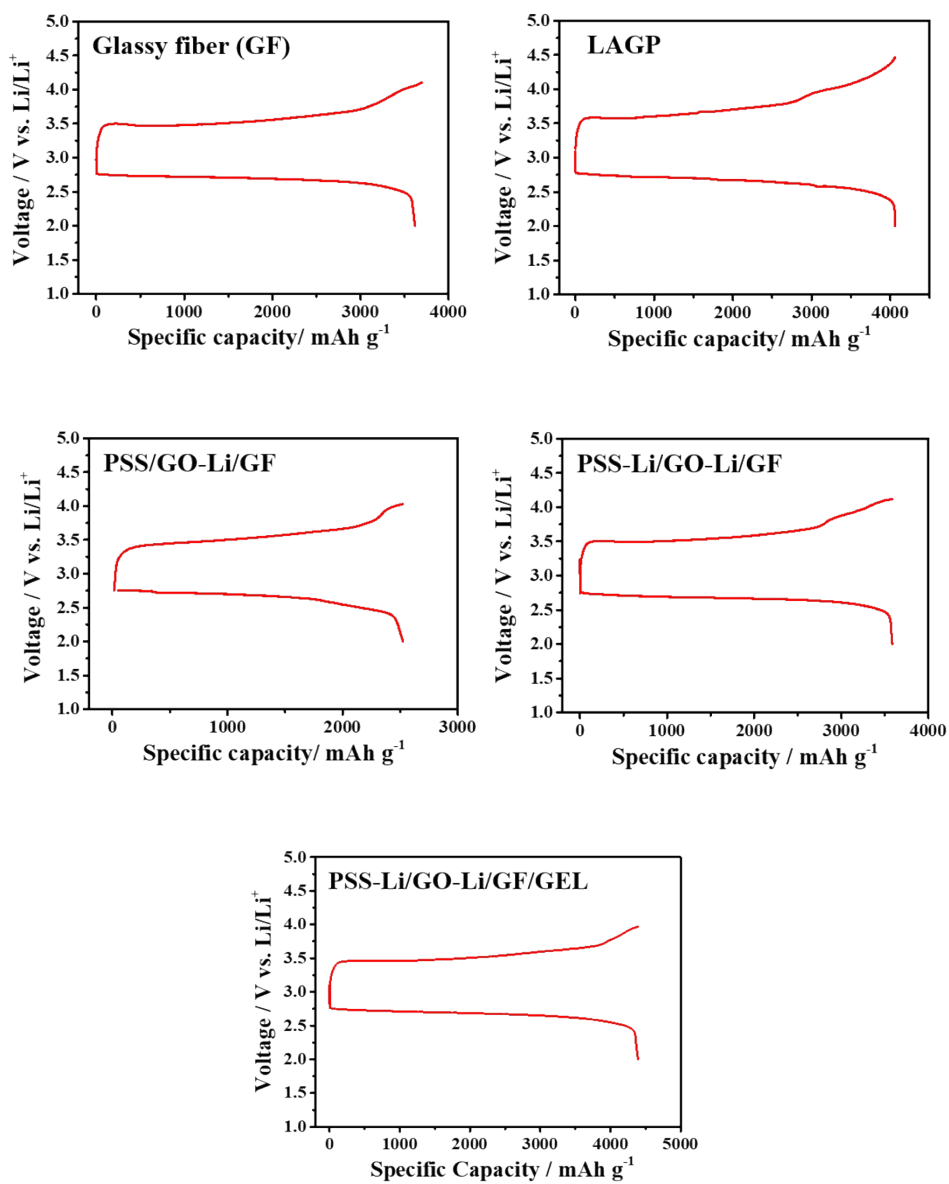


Figure S10 The full discharge/charge capacities of Li-O₂ batteries with different membranes

Figure S11

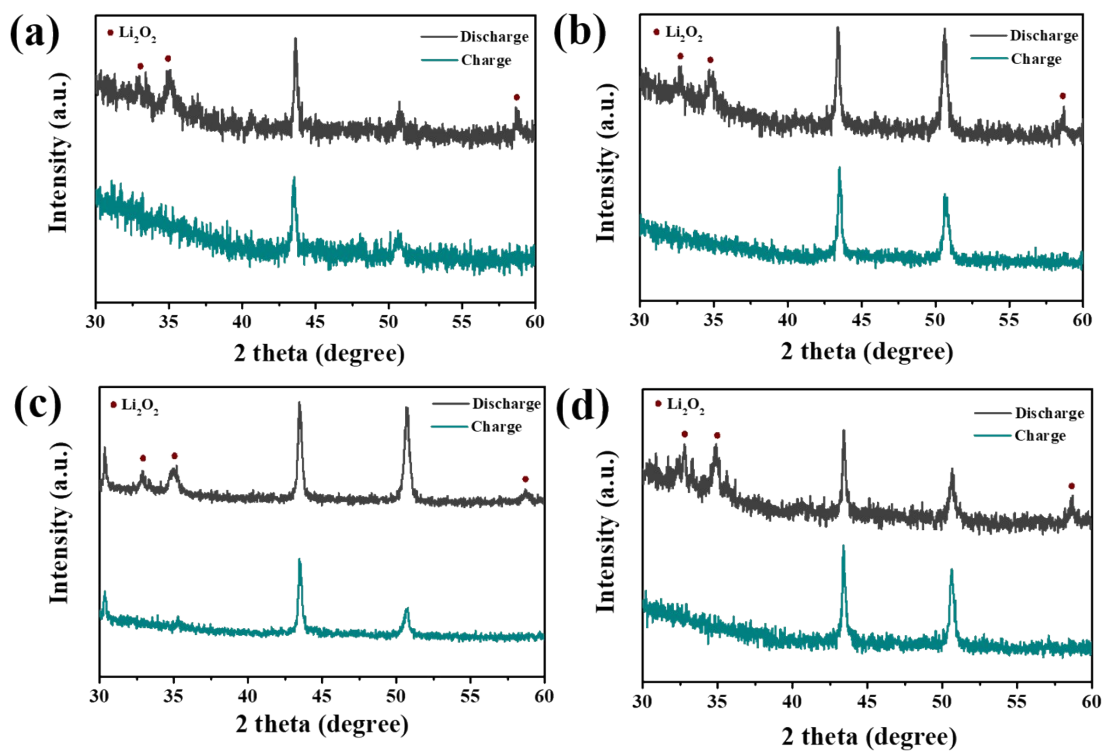


Figure S11 XRD patterns of the discharged products at the cathode after discharge and charge of Li-O₂ batteries with (a) LAGP membrane, (b) PSS/GO-Li/GF membrane, (c) PSS-Li/GO-Li/GF membrane and (d) PSS-Li/GO-Li/GF/GEL membrane.

Figure S12

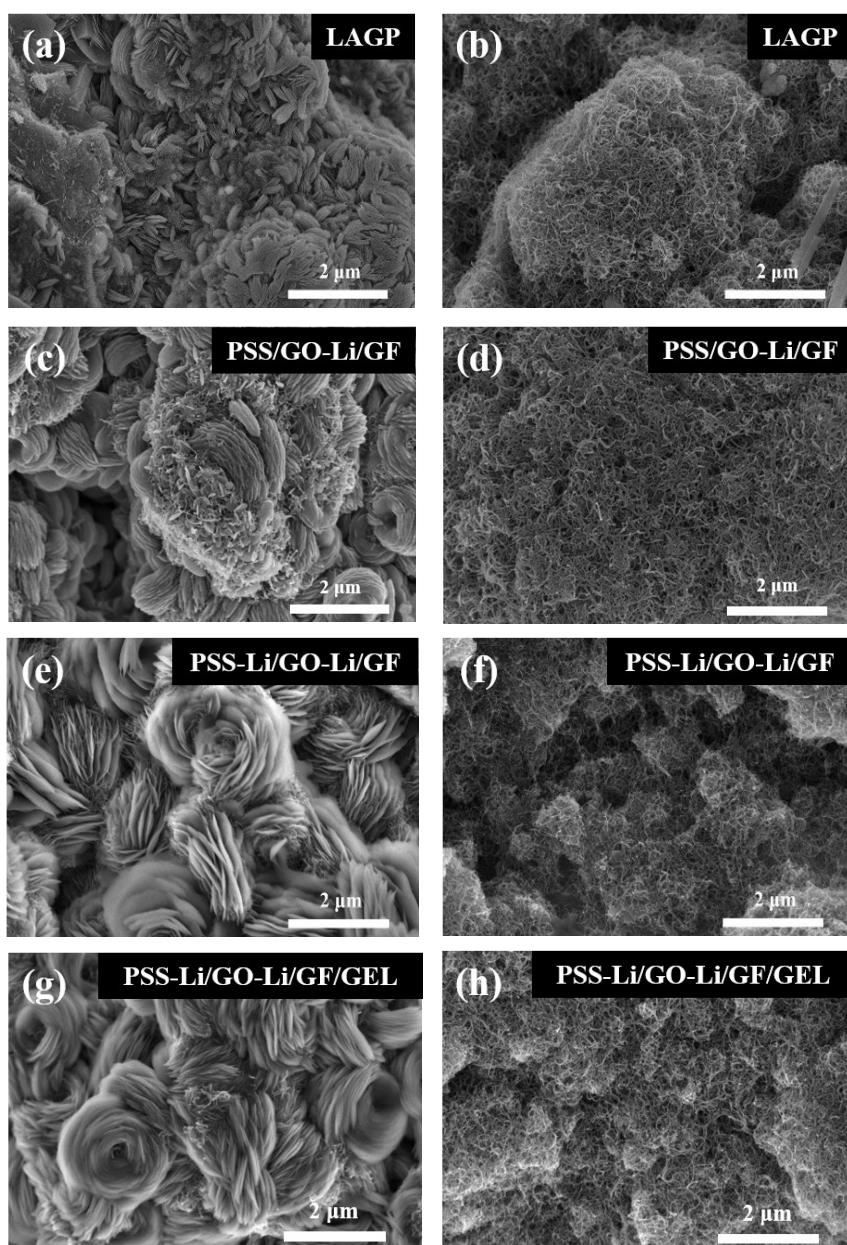


Figure S12 SEM images of discharged products at the cathode of Li-O₂ batteries with (a, b) LAGP membrane, (c, d) PSS/GO-Li/GF membrane, (e, f) PSS-Li/GO-Li/GF membrane, (g, h) PSS-Li/GO-Li/GF/GEL membrane.

Figure S13

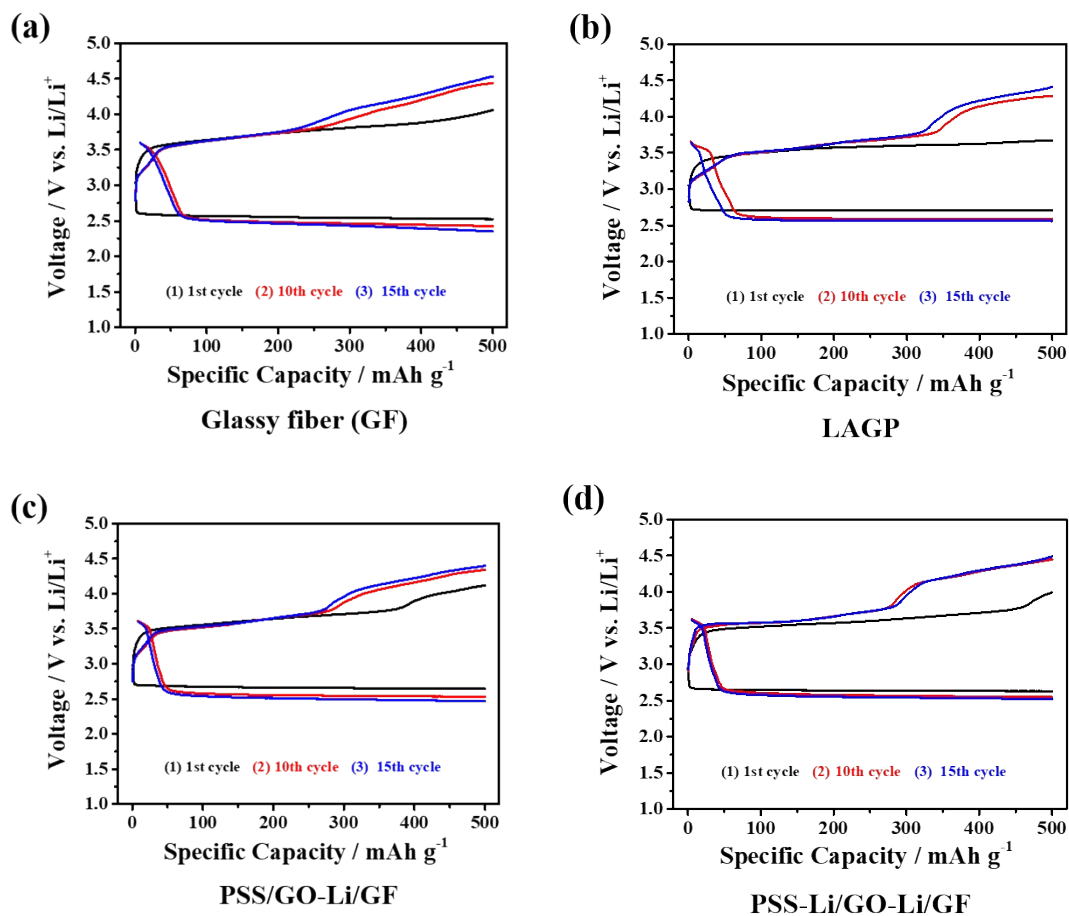


Figure S13 The 15 cycles performance of Li-O₂ batteries with (a) glassy fiber membranes, (b) LAGP membrane, (c) PSS/GO-Li/GF membrane, (d) PSS-Li/GO-Li/GF membrane at 400 mA g⁻¹ under a capacity cut-off of 500 mAh g⁻¹.

Figure S14

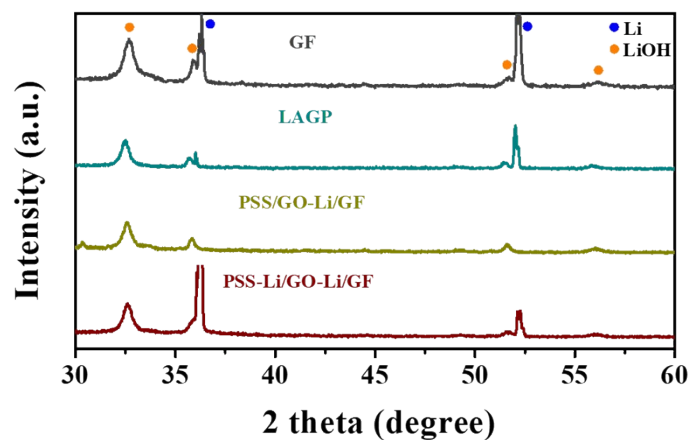


Figure S14 XRD patterns taken from Li-anodes with the protection of GF, LAGP, PSS/GO-Li/GF, PSS-Li/GO-Li/GF membranes after 15 cycles of Li-O₂ batteries.

Figure S15

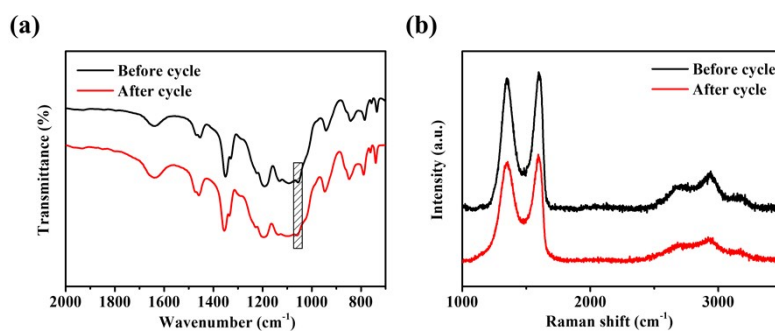


Figure S15 (a) FT-IR spectra of PSS-Li/GO-Li/GF membranes before and after cycles of Li-O₂ batteries. (b) Raman shift of PSS-Li/GO-Li/GF membranes before and after cycles of Li-O₂ batteries.

Figure S16

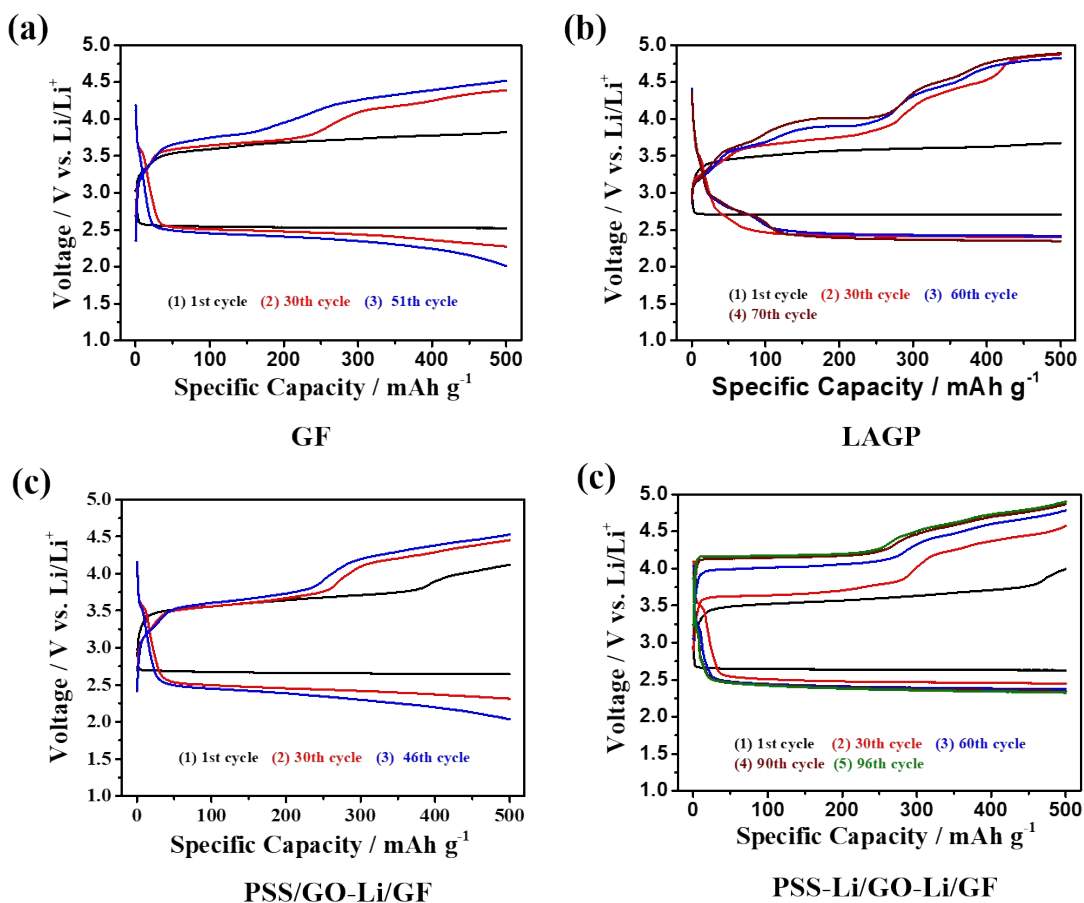


Figure S16 Cycling performance of Li-O₂ batteries with (a) Glassy fiber membranes, (b) LAGP membranes, (c) PSS/GO-Li/GF membranes, (d) PSS-Li/GO-Li/GF membranes at 400 mA g⁻¹ under a capacity cut-off of 500 mAh g⁻¹.

Figure S17

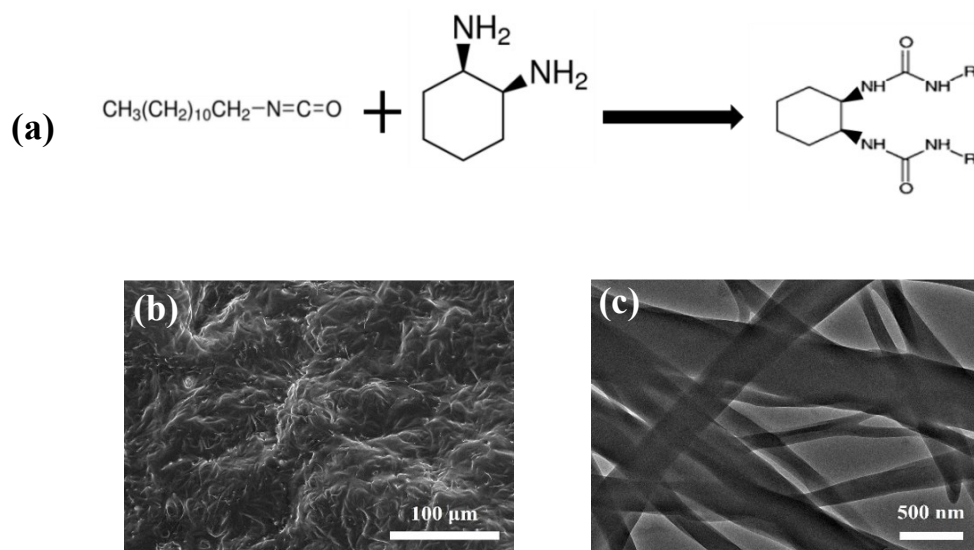


Figure S17 (a) The synthesis process of (S,S)-Dodecyl-3-[2-(3-dodecylureido)cyclohexyl]urea. (b) SEM and (c) TEM images of gel.

Figure S18

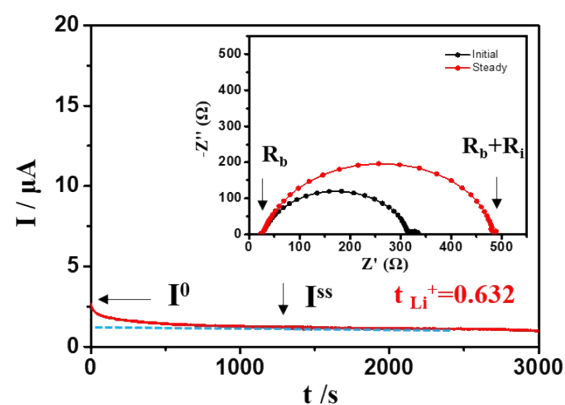


Figure S18 The chronoamperometry profiles of Li|PSS-Li/GO-Li/GF/GEL|Li cells tested under a polarization voltage of 10 mV (the corresponding EIS before and after polarization was provided in the inset graphs).

Figure S19

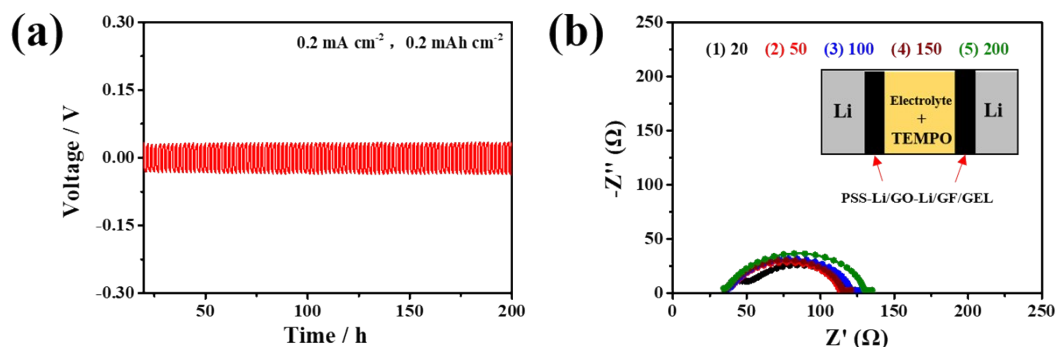


Figure S19 (a) Time-voltage polarization and (b) Nyquist impedance curves of Li|Li symmetrical cell with PSS-Li/GO-Li/GF/GEL membranes. The electrolyte of 2 M LiTFSI-TEGDME containing 0.25 M TEMPO were used.

Figure S20

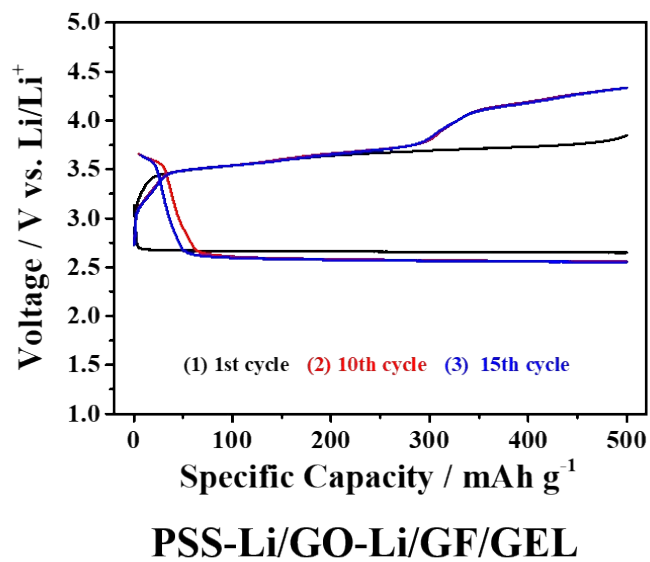


Figure S20 The 15 cycles of Li-O₂ batteries with PSS-Li/GO-Li/GF/GEL membranes at a current density of 400 mA g⁻¹ under a defined capacity of 500 mAh g⁻¹.

Figure S21

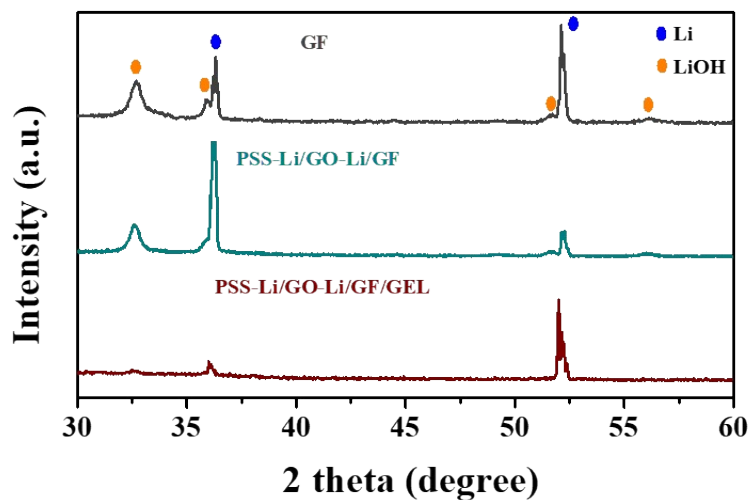


Figure S21 XRD patterns of Li-anodes with the protection of GF, PSS-Li/GO-Li/GF and PSS-Li/GO-Li/GF/GEL membranes after 15 cycles of Li-O₂ batteries.

Figure S22

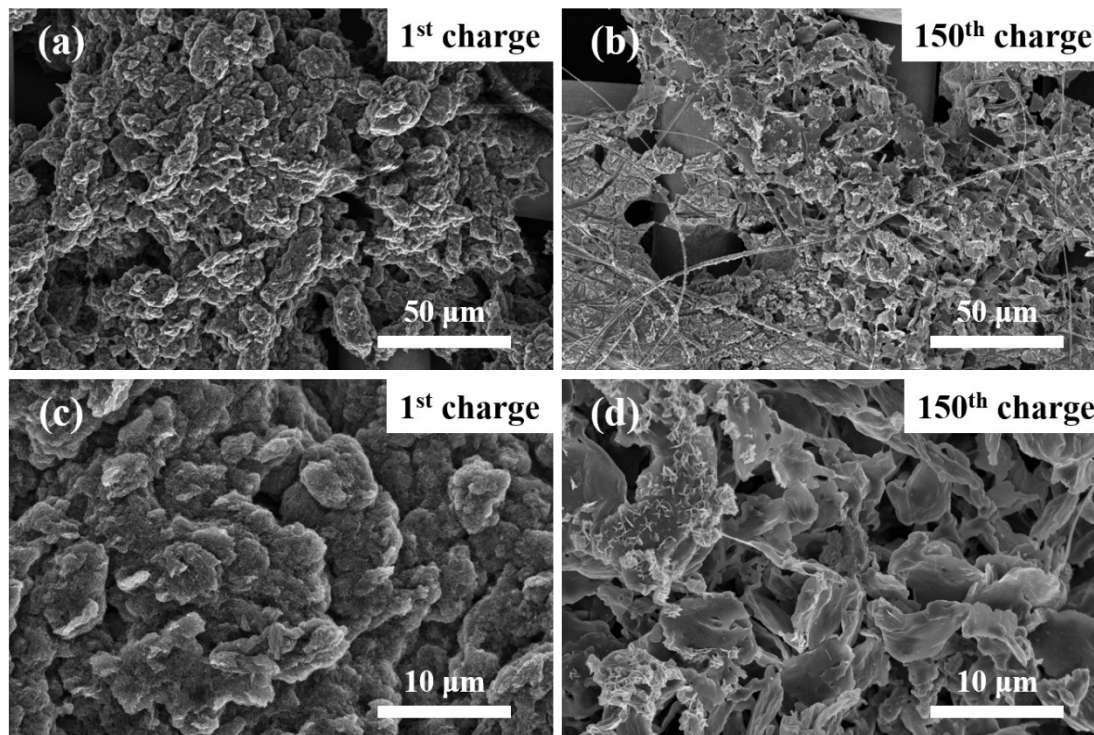


Figure S22 SEM images of before and after cycles at the cathode of Li-O₂ batteries with PSS-Li/GO-Li/GF membranes. (a, c) before cycles, (b, d) after cycles.

Figure S23 The cycle stability comparison of battery performance with the ever-reported and PSS-Li/GO-Li/GF membranes.

Year	Journal title	Cycle number	Capacity	Li Li symmetric cells	DOI
2017	Adv. Energy Mater.	90 th	600 mAh/g	138 h	10.1002/aenm.201602605
2017	Adv. Energy Mater.	100 th	1000 mAh/g	/	10.1002/adma.201701568
2017	ACS Appl. Mater. Interfaces	60 th	1000 mAh/g	250 h	10.1021/acsami.7b05466
2017	Nano Res.	43 th	0.75 mAh/cm ²	250 h	10.1007/s12274-018-1972-5
2018	Adv. Mater.	146 th	1000 mAh/g	900 h	10.1002/adma.201803270
2018	Adv. Energy Mater.	110 th	1000 mAh/g	/	10.1002/aenm.201702340
2018	Energy Storage Mater.	/	/	500 h	10.1016/j.ensm.2017.12.019
2018	ACS Appl. Mater. Interfaces	150 th	1000 mAh/g	240 h	10.1021/acsami.8b05393
2018	ACS Nano	50 th	1000 mAh/g	250 h	10.1021/acsnano.8b00348
2018	Small	40 th	0.75 mAh/cm ²	/	10.1002/sml.201801456
2019	Energy Storage Mater.	144 th	1000 mAh/g	/	10.1016/j.ensm.2019.01.009
2019	ACS Appl. Mater. Interfaces	/	/	900 h	10.1021/acsami.9b12634
2020	This work	150 th/375 th	500 mAh/g	1000 h	

Figure S24

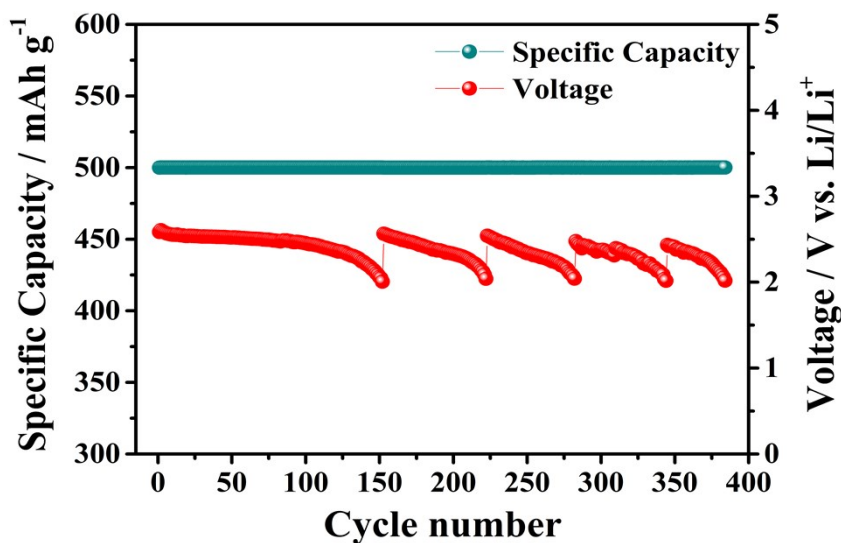


Figure S24 Cycling performance of Li-O₂ batteries with PSS-Li/GO-Li/GF membranes by replacing the cathode after cycle stop at 400 mA g⁻¹ under a capacity cut-off of 500 mAh g⁻¹.

Supporting References

- [1] R. Inada, K.-I. Ishida, M. Tojo, T. Okada, T. Tojo, Y. Sakurai, *Ceram. Int.* **2015**, *41*, 11136-11142.
- [2] D. Zhou, A. Tkacheva, X. Tang, B. Sun, D. Shanmukaraj, P. Li, F. Zhang, M. Armand, G. Wang, *Angew. Chem. Int. Ed.* **2019**, *58*, 6001-6006.